

METHODS FOR PASSIVE OPTICAL DETECTION AND RELATIVE NAVIGATION FOR RENDEZVOUS WITH A NON-COOPERATIVE OBJECT AT MARS*

Alan M. Didion,[†] Austin K. Nicholas,[‡] Joseph E. Riedel,[§] Robert J. Haw^{**},
and Ryan C. Woolley^{††}

Long-range passive optical detection of an orbiting inert sphere by a robotic Mars orbiter is investigated and trades are described in terms of detectability via reflected visible light in the presence of orbit uncertainty, gravitational perturbations, and camera electronics noise. A new approximate equation for signal-to-noise ratio (SNR) is developed to include most relevant camera imperfections, diffraction, and stray light from the Mars limb as relevant to this scenario. Using this method, a notional camera suite is designed to meet detection, navigation, and redundancy requirements for an example mission scenario. Results from a simulation tool demonstrate the long-range initial detection strategy in the presence of perturbations from various sources. Finally, navigation analysis shows that the information gathered using passive optical detection is sufficient to begin orbit matching.

INTRODUCTION

Inter-spacecraft cooperative rendezvous is routinely performed in Earth orbit, with the majority involving the resupply of the International Space Station (ISS) in Low Earth Orbit (LEO). These missions usually use some combination of communication between vehicles, Global Navigation Satellite System (GNSS) navigation, ground-based radar navigation, and near real-time monitoring from mission controllers on Earth. Rendezvous with non-cooperative artificial objects is rarely done in the civilian sector, but has upcoming applications in the field of orbital debris mitigation. In contrast, at Mars GNSS is unavailable, distances are much too great for Earth-based radar tracking, and the round-trip light time precludes extremely frequent and timely interactions with mission controllers. For these reasons, a passive optical detection and tracking solution is considered for Mars, despite not being among the more traditional sensing strategies at Earth.

* © 2018 California Institute of Technology. Government sponsorship acknowledged.

[†] Systems Engineer, Systems Engineering & Formulation, NASA/Jet Propulsion Laboratory, California Institute of Technology, 4800 Oak Grove Dr. Pasadena, CA.

[‡] Systems Engineer, Systems Engineering & Formulation, NASA/Jet Propulsion Laboratory, California Institute of Technology, 4800 Oak Grove Dr. Pasadena, CA.

[§] Principal Engineer, Mission Design & Navigation, NASA/Jet Propulsion Laboratory, California Institute of Technology, 4800 Oak Grove Dr. Pasadena, CA.

^{**} Navigation Engineer, Mission Design & Navigation, NASA/Jet Propulsion Laboratory, California Institute of Technology, 4800 Oak Grove Dr. Pasadena, CA.

^{††} Mission Design Engineer, Mission Design & Navigation, NASA/Jet Propulsion Laboratory, California Institute of Technology, 4800 Oak Grove Dr. Pasadena, CA.

Sample return missions from the surface of a planet will, in all probability, require mission and campaign-level staging in order for the sample container to make the round trip. Much like Apollo, one attractive option is to launch the samples into low orbit and have an orbiting robotic spacecraft rendezvous with them for later return to Earth. This paper explores a Mars Sample Return (MSR) concept where the sample container is fully passive and then examines the implications that would have on the sensor complement and approach strategy of the rendezvous and return spacecraft. In the vernacular of this investigation, the orbiter is referred to as the Sample Return Orbiter (SRO) and the inert orbiting sample container is referred to as the Orbiting Sample (OS).

The rendezvous strategy of a potential robotic orbiter with an inert object in Mars orbit can be divided into four primary phases. These include:

1. Initial acquisition. The orbiter searches a pre-defined area of space in a pre-sequenced manner to obtain visual detection of the object, as defined by orbital element statistical distribution predictions or other a priori knowledge. This occurs at long range and ends with successful confirmation of the object and estimation of its orbital elements. Additional measurements can be performed until the navigational errors are sufficiently small to begin coarse orbit matching.
2. Orbit matching. Analysis of the relative orbits has been completed and commands are sent from Earth to the orbiter to begin maneuvers to eliminate drifts in relative orbital elements and close the separation to a safe standoff orbit.
3. Approach and inspection. Short-range cameras can be used for visual inspection of the object from a safe distance before beginning terminal rendezvous.
4. Terminal rendezvous. Upon go/no-go command from Earth, the orbiter autonomously closes the final distance in the safest manner possible for docking or capture.

The investigation described herein will focus primarily on the initial acquisition phase and meeting the transition requirements to begin the orbit matching phase, with some discussion of navigating the approach, while detail of the subsequent phases will be left to subsequent publications.

A major conclusion of this investigation is that current optical camera technology is sufficient, even under conservative camera noise and object albedo assumptions, to safely begin orbit matching maneuvers without need for a cooperative radio interface or other action on the part of the object. The required optical camera suite can make use of existing technology and is modest in mass and power draw. The suite can provide the required orbit determination of the target with only a few hours of observations. Further, it is found that the system can be operated with ground-in-the-loop involvement during long-range initial detection and that novel autonomy in this regime is not required. Finally, a "lost-in-space" case is presented to discuss contingency scenarios. The information presented about potential Mars sample return is provided for planning and information purposes only.

SIGNAL-TO-NOISE RATIO

At long ranges, the key problem is whether the camera(s) observing the OS are capable of detecting its presence. It is, after all, a small object (< 30 cm diameter) at very great distance (>3,000 km). For perspective, this is like standing in Los Angeles and taking a photo of a bowling ball in Chicago, albeit backlit by the blackness of space. While this sounds daunting, this investigation will show that indeed existing modern cameras are more than capable of such a feat.

An accurate equation for signal-to-noise ratio (SNR) is integral to the following simulations, and so a new equation was developed to include most relevant causes of error and noise in this

environment. In previous work on this topic, Woolley et al proposed an equation for SNR of the OS in the camera detector.¹ This equation is repeated below as Equation (1), with nomenclature adjusted to match the rest of this paper as closely as possible:

$$SNR = \frac{\pi d_{ap}^2}{4} f t_e * \left(\frac{\pi d_{os}^2}{4} * \rho \right) * \frac{1}{r^2} * g(\phi) \frac{kE}{N} \quad (1)$$

Where the phase function:

$$g(\phi) = 10^{-0.01\phi} \quad (2)$$

Each symbol is defined in the “notation” section at the end of this paper. This equation is a good starting place, but had a few issues such as an inaccurate phase function, lack of apparent motion (smear), and a consolidated noise term, which could not be used to describe the higher-fidelity noise sources desired here. Instead, a phase function for a diffuse sphere was used (ensuring phase angle is used in degrees), as shown in Equation (3).

$$g_{diffuse}(\phi) = \frac{2}{3\pi^2} \left[\sin \phi + \left(\pi - \phi * \frac{\pi}{180^\circ} \right) \cos \phi \right] \quad (3)$$

It should be noted that the diffuse sphere phase function is sometimes defined differently with respect to the SNR equation, specifically that the π term in the denominator often cancels with one of the π terms in the SNR equation. This form is chosen so that the SNR equation can be explained simply in terms of areas and ratios and $g(\phi)$ is the amount of light reflected in a given direction, as a fraction of the total light incident upon the entire surface. The maximum value of the diffuse sphere phase function is 0.212, if the viewer is observing the sphere at zero phase angle. This means that roughly 79% of the light is scattered away from the direction of the incoming light due to the surface shape and material reflectance properties.

More insight was desired into the noise terms to better understand the sources of noise and how they change with variables of interest. In this case, there are four main noise contributors: shot noise, dark current noise, read noise, and stray light noise. The dark current and read noise are camera parameters for specific hardware. It should be noted that camera noise is generally quite sensitive to temperature, but for the purpose of this analysis, a worst-case temperature was chosen based on the foreseen thermal design and noise parameters for that situation. The stray light model was noted to be one of the largest areas of uncertainty for this phase. To give the most realistic model possible, flight data from the Mars Reconnaissance Orbiter (MRO) Optical Navigation Camera (ONC) was examined. In many of the images, stray light noise from Mars obscures the fainter background stars. Using these images, an empirical model quantifying the stray light noise, and scaling it to other imaging situations was derived. This is shown in Equation (4):

$$N_{stray}(\psi, t_e) = 0.871 * d_{ap}^2 * t_e * e^{-2.8\psi} \quad (4)$$

The root-sum-square (RSS) of these noise terms combines them into a single noise term, shown in Equation (5) along with the method for counting pixels smeared due to relative angular motion.

$$N = \sqrt{P_{px}\eta + N_{dark}t_e + N_{read}^2 + N_{stray}^2} , n_{px} = \max\left(1, \frac{at_e}{\theta_{px}}\right) \quad (5)$$

Now, all the terms can be assembled into one equation for SNR, Equation (6):

$$P_{px} = P_{sun} * \frac{\pi d_{os}^2}{4} * \rho * g(\phi) * \frac{1}{r^2} * \frac{\pi d_{ap}^2}{4} * \frac{1}{n_{px}} * t_e , SNR = \frac{P_{px} * \eta}{N} \quad (6)$$

The predictions from this form of the equation were shown to be in agreement with MRO ONC historical data, but in-depth laboratory verification and validation would be required in later phases to fully vet this formulation.

It should be noted that two additional effects, jitter and saturation, were not included because they are not dominant effects at present, but they could be added in the future. It was also recognized that an OS streaking across multiple pixels would be easier to detect than a single pixel of the same SNR. Therefore, the “detectability” metric is introduced in Equation (7). If the detectability is greater than or equal to unity, the OS is considered detectable.

$$detectability = \begin{cases} n_{px} = 1 & SNR / 5 \\ 1 < n_{px} < 5 & SNR / (-0.5n_{px} + 5.5) \\ n_{px} \geq 5 & SNR / 3 \end{cases} \quad (7)$$

CAMERA SUITE FOR OPTICAL DETECTION

This section presents a single suite of optical cameras that support sensing needs from initial acquisition through terminal phase. The needs of the various phases are very different:

- **Initial Acquisition:** infrequent images (a few per hour) at very low brightness. Initial position knowledge very low, so a reasonably large field of view is needed. Accuracy on the order of a few hundred meters is sufficient to start orbit matching.
- **Orbit Matching:** very infrequent images (a few per day) at low brightness, but with better initial position knowledge than acquisition such that it is almost certain to be in field of view. Accuracy increases over time with many observations
- **Approach and Inspection:** infrequent images (a few per hour) at high signal. Initial position knowledge is good, the goal is to increase precision for terminal phase. OS will subtend multiple pixels at this range.
- **Terminal Rendezvous:** frequent images (multiple images per minute) at very high SNR. Initial position knowledge is excellent and (aside from fault conditions) almost certain to be in field of view. The OS is resolvable as a multi-pixel shape below ranges of tens of km, allowing multi-pixel image centroid finding. Accuracy on the order of centimeters is needed for capture. This loop is closed in real time, autonomously.

It is apparent that the camera needs of the orbit matching phase are very similar to the initial acquisition phase, though at different cadence and with different a priori conditions, and that the approach and inspection phase has needs that mix acquisition and terminal phase needs. Therefore, a first step is examining the needs of the two bounding phases separately. A camera designed for the purpose of long range detection is denoted as the “Narrow Angle Camera” (NAC) and one for the purpose of terminal rendezvous the “Wide Angle Camera” (WAC), differentiated here by field of view. A sensor of intermediate performance is termed the “Medium Angle Camera” (MAC).

Another primary concern is redundancy. Sample return missions are typically risk averse, so it is assumed here that the camera suite must be robust to the complete failure of any sensor. Because no single sensor could be found which adequately services the needs of both long- and short-range phases, there are an absolute minimum of four sensors: two NACs and two WACs, where one of each is redundant, and where the NAC can successfully navigate the spacecraft into WAC range.

For the NAC, there is a lower bound on the field of view due to a combination of spacecraft slew/settle limits and the number of images needed per orbit for navigation. In some work outside

the scope of this paper, it was shown that a field of view of roughly 5-deg minimum is required to facilitate possible search mosaicking and limit its required duration.

For the WAC, the driving needs are for a large field of view, and excellent accuracy at very close minimum range to facilitate delivery to the capture system. It was determined that using stereo would be the most robust and most accurate solution for the terminal rendezvous, especially given the relatively large baseline of ~1.5 m which could be accommodated on the spacecraft bus. This means two cameras are required to be functional, meaning three total WACs are included for single fault tolerance.

A MAC was considered to bridge the gap between NAC and WAC useful range. The MAC offers a compromise in between the NAC and WAC to help bridge the gap. However, it was considered undesirable to add two cameras just to make this transition robust, because it could plausibly work with two NACs. Therefore, the redundant NAC was replaced with a single MAC, with the suite retaining one failure tolerance. The overall specifications for the three cameras are summarized in Table 1.

Table 1. Requirements for the Example Camera Suite.

Sensor	Max Range	Min Range	FOV	Aperture	Accuracy of OS Centroid
NAC	>3,400 km	< 100 m	> 5°	< 10 cm	Angular: < 35 μ rad
MAC	>1,000 km	< 10 m	> 10°	< 5 cm	Angular: < 500 μ rad
WAC	>1 km	< 0.25 m	> 60°	< 5 cm	Angular: < 1 mrad Range: ~15 cm @ 10 m

As an exercise and proof of concept, an example hardware concept was assembled using in-house JPL designs. The most applicable design was based on the Mars 2020 EECAM family.² The Mars 2020 rover will have nine cameras of this family onboard. All cameras use identical electronics but have three different optics configurations. Table 2 contains the parameters for the example camera suite. A similar design approach was followed here: all three cameras use the heritage EECAM electronics and have optics that match the function. The WAC is actually a black-and-white version of the M2020 NavCam, with no other changes needed. The NAC requires a fairly large telephoto lens and is clearly the most massive component of the camera suite. The total suite current best mass estimate is around 6 kg.

Table 2. Example Rendezvous Camera Suite Parameters.

Sensor Capabilities	
Type	20M Pixel CMOS Image Sensor
Array Size	5120 x 3840
Pixel Size and Pitch	6.4 μ m ² on 6.4 μ m Pitch
Shutter	Global
Pixel Quantization	12 bit, Monochrome
Electronics Mass	0.43 kg
Electronics Volume	65 mm x 75 mm x 55 mm

Optics Configurations				
Camera	Field of View	f/#	iFOV	Optic Mass
WAC x 3	95 x 71 deg	f/12	≤ 320 urad/pix	0.25 kg
MAC x 1	14 x 11 deg	f/2.8	≤ 50 urad/pix	0.37 kg
NAC x 1	9 x 7 deg	f/2.2	≤ 30 urad/pix	2.5 kg

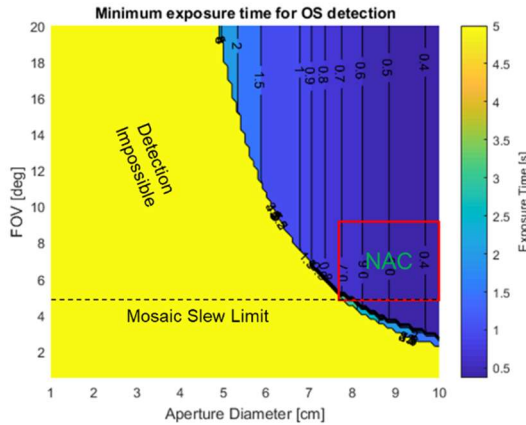


Figure 1. The design space of the NAC. The camera was decided to be approximately 10 cm aperture diameter and 7 deg FOV; detection possible at 3,400 km (longest chord at this altitude).

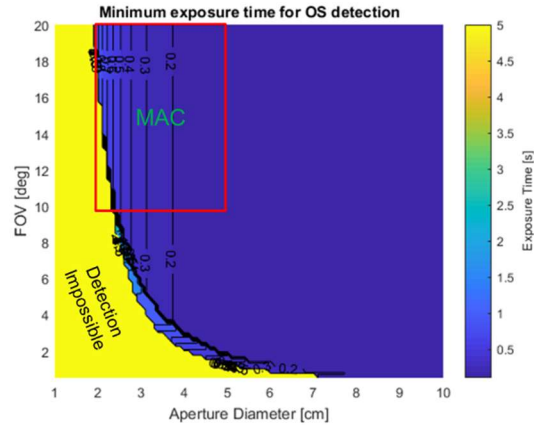


Figure 2. The design space of the MAC. The camera was decided to be approximately 4 cm aperture diameter and 11 deg FOV; redundant detection possible at >1,000 km.

A tradespace analysis was performed to determine the valid design space for the NAC and MAC, Figures 1 and 2 show the results in terms of necessary exposure integration time to achieve detection. The yellow plateaus represent regions where the relative motion of the OS across multiple pixels and/or camera electronics noise wash out the signal, making detection impossible (infinite required exposure time). The NAC is designed to be capable of detection at maximum range, the line-of-sight distance where the chord connecting the OS and the SRO intersects the martian limb, or about 3,400 km. MAC initial detection is only for redundancy, so its requirement is relaxed to 1,000 km.

OPTICAL DETECTION SIMULATION

An analytical model was developed to propagate the system through time, including n-body gravitation and aspherical potential effects. At each step, relative range, azimuth, elevation and solar phase angle are computed and eclipses and occultations are identified. SNR is computed for the given camera characteristics and orbital geometry and plotted over time. The above radiometric analyses, camera parameters, and orbital propagator have been incorporated into a comprehensive MATLAB tool known as the Mars Orbiter Initial Acquisition for Rendezvous Application (MOIRA) to facilitate broad trades and comparisons to support pre-phase-A design activities. In particular, the tool was key in demonstrating the feasibility of the optical detection scenario and exploring sensitivities to given inputs such that requirement boundaries could be identified. The benefit of MOIRA's instantiation as an integrated MATLAB tool manifests in the elimination of legacy processes such as the manual handling and checking of spreadsheets and stand-alone models which were time consuming and error-prone. Additionally, MOIRA can be loaded with inputs or

wrapped to run batches of multiple input sets, and run in the background or overnight, saving outputs automatically and making significant use of parallel computing.

Inputs & Assumptions

While there is a broad design space to be explored in this problem, this paper will discuss a particular example case and its performance in a vacuum. The case chosen can be described by the following set of inputs and assumptions about the orbit of the SRO (Table 3), the insertion state distribution of the OS, and its physical parameters, discussed next.

Table 3. Ideal Keplerian Orbital Elements of the Potential Mars Orbiter in the MarsIAU Coordinate Frame.

Element	Symbol	Value	Unit
Semi-Major Axis	a	3,865.8	[km]
Eccentricity	e	0	[N/A]
Inclination	i	25	[deg]
Solar Beta Angle	β	90	[deg]

OS Insertion State Dispersions

The assumed OS would be launched to low Mars orbit via a Mars Ascent Vehicle (MAV) multi-stage rocket. Due to the in-flight performance of the MAV propulsion, guidance, and control, there would be some uncertainty on the OS's initial orbital state. These dispersions can be predicted at a variety of fidelity levels; for this analysis, a simplified covariance model was constructed by fitting to MAV Monte Carlo results, in order to facilitate simulation.³ Summary 3σ statistics on the delivery using this model are shown below in Table 4. Note that apoapsis, periapsis, and eccentricity are not normally distributed, so these are the 99.7 percentile bounds. The rest of the variables are well modeled by the normal distribution.

Table 4. 3σ Statistics on MAV Dispersions Using a Covariance Model.

a	e	Apoapsis	Periapsis	inc	RAAN	Arg. of Latitude	Alongtrack
± 32 km	< 0.019	-2 to +106 km	-97 to +2.4 km	$\pm 1.1^\circ$	± 0.17 deg	± 0.71 deg	± 46 km

The nominal MAV launch would place the center of the OS distribution with semi-major axis (SMA) 32 km lower than the SRO, and 35 deg trailing in true anomaly, generating an expected mean OS state that begins at 2,340 km line-of-sight range and drifts toward and under the orbiter shortly after insertion. This geometry affords an excellent opportunity for imaging the OS with a small field of view camera. The OS "cloud" distribution is generated by randomly sampling the expected OS means and deviations (based on assumed MAV parameters) when MOIRA starts, creating a Monte Carlo scenario with many OS initial states. These will all behave differently in the relative orbital dynamics due to their starting locations. In the case described here and shown in plots, 50 initial states were generated. MOIRA is designed to evaluate the capability of a given design to detect and track the OS regardless of its initial state within the 3σ dispersions.

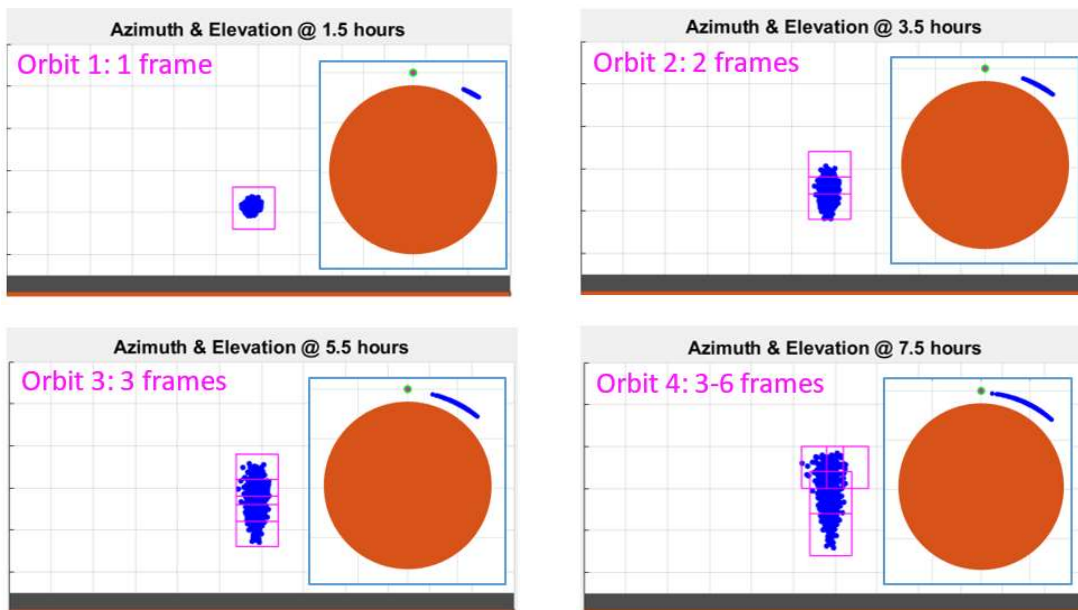


Figure 3. Apparent Evolution of the OS Distribution as seen from the SRO vs. Time, with Inset Relative to Mars in and Orbital Rotating Frame.

Examination of the geometric properties of the distribution vs. time, as in Figure 3, one can see the cloud of potential OS locations remains within a single 5 deg by 5 deg field of view for the first orbit. After four orbits, the OS cloud has grown to subtend four frames, and would require a simple mosaic to cover.

Orbital Dynamics

The orbital dynamics are propagated numerically in MOIRA via MATLAB's ode113 function, a non-stiff ordinary differential equation integrator, utilizing adaptive time-step sizing, n-body gravitation (namely Jupiter and the sun), and a $J_{3,4}$ Martian gravity field. MOIRA is also capable of including atmospheric drag and solar radiation pressure, but these effects are neglected for this investigation primarily due to their small effects their relatively large increase to MOIRA's computational demand. Prior to beginning analysis, MOIRA uses SPICE to obtain the Earth and Sun ephemerides relative to the MarsIAU frame over the analysis period specified. The OS initial state distribution is then sampled, and each OS instance is propagated and the radiometry and occultation/eclipse analysis is done through parallel computation before being recombined for plotting and saving.

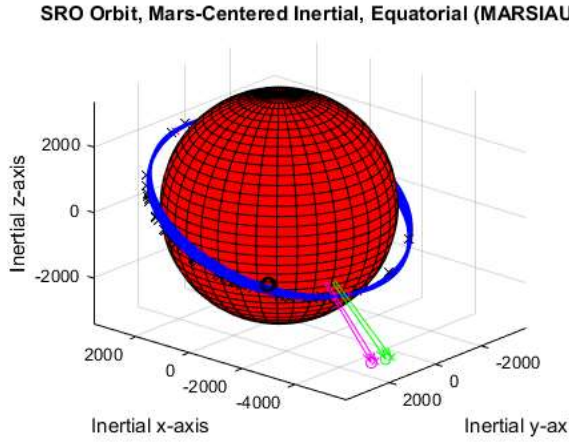


Figure 4. The geometry of the problem relative to Mars (red), Earth (green), and the sun (magenta).

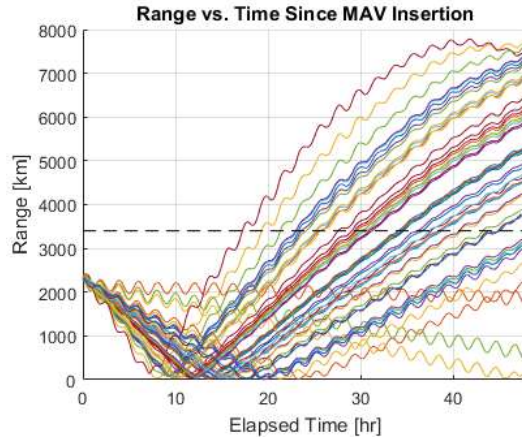


Figure 5. The distribution of initial insertion states causes the OS “cloud” to spread over the course of the analysis period. Colors consistent with Figure 8, dashed line is the maximum chord (3,400 km).

While the primary output of MOIRA is the tabulation of SNR vs. time, Figure 4 shows a three-dimensional representation of the orbital geometry to aid intuition and communication. Here, the blue curve shows the orbiter’s trajectory over the analysis period of 48 hr and the black circles and black crosses represent the respective initial and final dispersions of the OS. Note that in only 48 hr, the possible locations of the OS have drifted apart to encompass all 360 deg of true anomaly. The green vectors show the starting and ending direction of Earth, and likewise magenta, the sun. See also Figure 5, which shows the relative line-of-sight range from SRO to OS vs. time. One can observe behaviors on three time scales: relative motion on the scale of the orbital period, diffusion of the OS distribution due to their differences in SMA, and a third much longer-period diffusion due to orbital precession. The latter does not come into play in this scenario, as the SRO should be in-place and ready for detection when the OS is inserted into orbit. If it were not present and instead arrived after a period where this effect is relevant, the SRO would find itself in a “lost-in-space” contingency scenario, which is described briefly later in this paper.

Note that some OS instances approach the SRO very rapidly, due to a particularly low SMA value, while others with elements particularly similar to the SRO nominal state have very slow approach rates. The latter cases may be troublesome in their tendency not to approach within comfortable detection range for some time after insertion, but the relative orbital geometry was designed such that the expected distribution would not yield an OS which recedes from the orbiter, never reaching detection range. The colors used here are consistent with the SNR vs. time shown later in Figure 8; make note of the bright red outlier which quickly approaches and passes under the SRO in about 8 hr elapsed time.

Radiometry

A key requirement for the optical detection scheme was identified: the camera must attain sufficient SNR to effect detection when the OS is at a solar phase angle of 90 deg (half-moon) or less while at detection range. The SNR required (Equation (6)) to effect detection was set at 5 for static detection, and 3 for a multi-pixel smear. Figure 6 shows the SNR and detectability as a function of OS solar phase angle. For reasons to be described in the next figure, “detectability” is defined as the achieved SNR normalized by the required SNR to effect detection, and >1 indicates successful detection of the OS. One can see that the NAC design, in-situ with the problem geometry, is capable

of achieving the static SNR required at phase angles >90 deg (indeed > 120 deg) at this given range of 2,340 km.

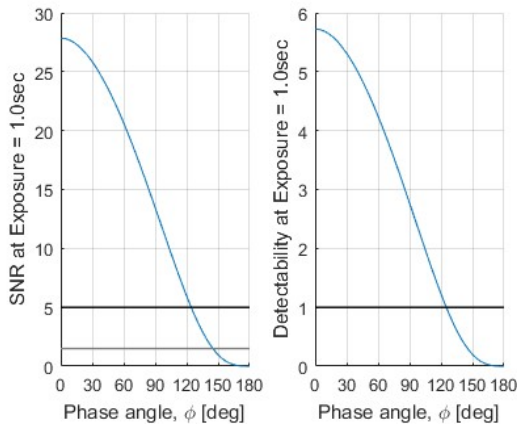


Figure 6. The notional NAC designed for this application was shown to be capable of achieving static detection (SNR > 5 , detectability > 1) at a phase angle of 90 deg and greater at a range of 2,340 km.

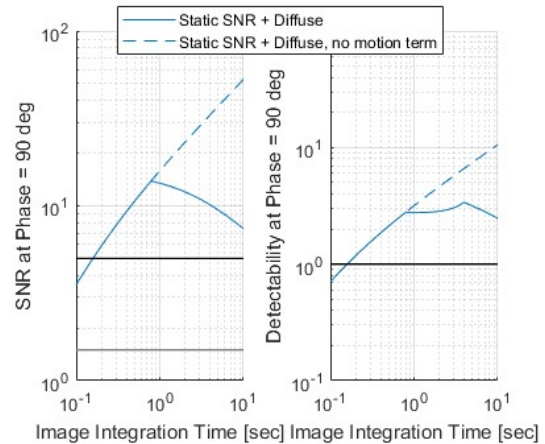


Figure 7. There exists a predictable optimal integration time to achieve peak SNR and detectability of the OS at half-moon in the presence of relative angular motion and electronics noise.

On the right, Figure 7 shows how the NAC SNR and detectability vary with exposure time, with and without including the effects of relative angular motion. The OS and SNR are moving relative to one another, and the relative angular motion cannot be fully known or accounted for by the SRO, so the OS’s image can be expected to smear across multiple pixels if the exposure time is long. To an extent, this smearing is helpful as it reduces the required SNR to effect detection (multiple SNR > 3 pixels in a line can stand in for one SNR > 5 pixel, see Equation (7)), and one can see an area with an increase in detectability despite decreasing per-pixel SNR. However, if the image smears across many pixels without having time to deposit enough signal in them to effect detection, the signal will be drowned by optical and electronic noise. Therefore, a “sweet spot” exists, dependent upon camera specifications and range, but generally at around 1-5 seconds of exposure. Note that shorter range would mean increased SNR but also increased relative angular motion. This short-range regime is not considered here because initial detection is done at long-range, and the relative angular motion of the system should be known and can be cancelled (via slewing) during subsequent observations.

Results

The ultimate output of MOIRA is a time-series of SNR for each possible OS state as it is propagated through the scenario. From this, one can determine the suitability of the camera design, orbital geometry, and OS element distribution for a given case, and make observations and adjustments which feed back into the iterative design of the rendezvous initial acquisition phase.

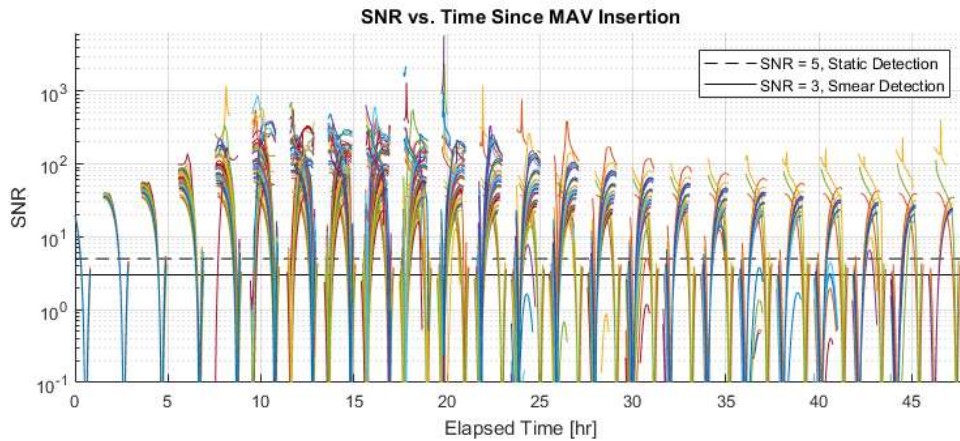


Figure 8. SNR vs. time for the distribution of possible OS trajectories relative to the SRO.

From Figure 8, and via analysis of the underlying tabulated data, one can ascertain a few key pieces of information about the case in question. The first key result is that the SNR achieved at initial range is likely sufficient to effect detection, but does not necessarily meet the detection SNR requirement (90 deg phase angle) for a few hours after insertion. One can also see both short-term and long-term behaviors in the distribution over time, and can compare the behavior of the bulk to the behavior of the outliers. One can see immediately the phase-angle behavior, as the SRO and OS orbit Mars together and the sun's relative position cycles. Because the SRO leads the OS in their orbit, they exit eclipse with the sun opposite the OS with respect to the SRO (low solar phase angle, high SNR), and enter eclipse with the OS mostly backlit by the sun (high solar phase angle, low SNR).

One can also see periodic gaps in the SNR data when the OS is in eclipse, which is handled in MOIRA by zeroing SNR for any time step during which the angle between Mars and the sun as viewed from the OS is less than the apparent angular size of Mars at the current altitude. Occultation of the OS by Mars is handled in the same manner, and this effect can be seen in the thinning of the later data as some OS instances recede over the Martian limb ahead of the SRO. In general, the distribution for this case remains fairly coherent until about 8-10 hr have elapsed and some states have approached rather close, gaining SNR boosts from decreased range but also scattered-light penalties for their angular proximity to the limb. After this period has elapsed, the distribution has grown large and will require significant mosaicking to cover, so it is desirable that the SRO's NAC would be capable of effecting detection prior to this point.

Note the bright-red outlier from Figure 5, which was the first OS instance to pass under the SRO at approximately 8 hr elapsed time. Here, we can see that same case as it breaks from the group and is the first to pass under the SRO, where its SNR suffers greatly as it is backlit by Mars. It then proceeds ahead of the SRO and eventually is the first to pass over the Martian limb, into occultation. This case then becomes the challenging case for the scenario, driving the SRO's detection scheme to be capable of detecting the OS before these events occur to determine its orbital parameters for subsequent observations or to begin computations for orbit-matching maneuvers.

Armed with these results, one can determine that optical detection in this environment would be feasible, and experiment with various optical suites and problem geometries to better inform design before moving on to assessing the navigational adequacy of these observations.

RELATIVE NAVIGATION WITH OPTICAL OBSERVATIONS

OS State Determination

The SNR plot (Figure 8) shows that initial acquisition of the OS could be performed comfortably in the first few hours after orbit insertion. Camera capability would therefore be adequate for determining initial orbit parameters. Figure 9 shows that neither NAC nor MAC camera uncertainty will contribute significantly to orbit uncertainty. The two elements most sensitive to the rendezvous procedure are shown: semi-major axis and inclination. Both show high fidelity capability of determining orbit parameters.

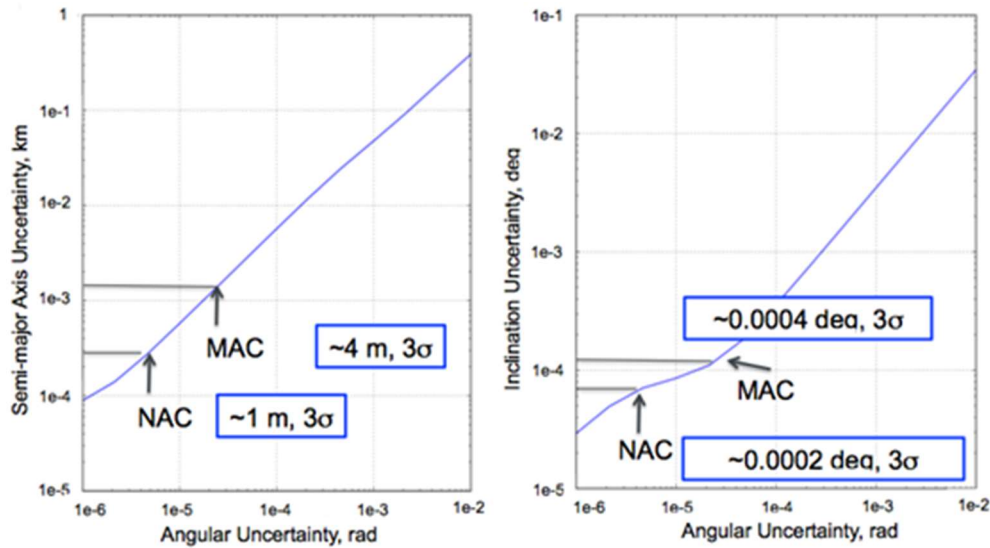


Figure 9. Orbit uncertainty vs. optical measurement uncertainty (1σ). OS observed for 10 hr, semi-major axis (left), inclination (right).

A navigation model of initial OS detection was built using the center of the OS distribution as the nominal location for the OS. Two-way range-rate tracking data and 6 NAC images per hour are simulated in the model, with the strategy being to accumulate data until the initial OS position dispersion evolves to fill up a field-of-view. Range-rate tracking from the orbiter is acquired continuously when it is in view of a ground station; NAC optical navigation images of the OS are also acquired continuously except when the OS is in eclipse, in occultation, or when the sun-OS-orbiter angle exceeds 90 deg (half-moon). The OS is in view of the orbiter for approximately 2 out of every 6 days; during the other 4 days it is occulted by Mars from the orbiter's view. The OS also experiences 12 solar eclipses per day (Figure 10).

During initial acquisition, image processing is performed manually (on Earth) in order to verify data quality and because the timeline allows it. For the earliest images, a 5-hr latency is presumed between data retrieval and the orbit determination solutions; that delay decreases to 2 hr with expected process improvement.

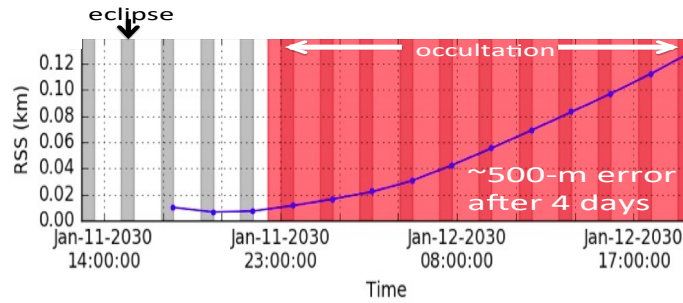


Figure 10. OS state prediction uncertainty (1σ).

Analysis indicates that the OS orbit would be well-determined within 7-10 hr of initial detection, with OS position known to 20 m, 1σ . The timespan for these observations fits easily between occultations. Moreover, orbit knowledge is robust and does not degrade significantly during occultations, meaning the OS will be close to its expected location when emerging from occultation. Although the NAC FOV is not wide enough to ensure OS acquisition within a single frame after it emerges from occultation, an elementary 3x3 mosaic can be applied to re-acquire it (Figure 10). Orbit knowledge with this level of fidelity and reproducibility is sufficient for the SRO to begin orbit-matching activities with the OS. Model assumptions can be found in Appendix A.

Relative Navigation Suitability for Closing Operations

After orbit matching, the SRO would have to begin autonomous terminal rendezvous while tracking the OS optically. A simulation was created using a close model of the simplified AutoNav filter to determine the preliminary suitability of this scheme for the later terminal rendezvous phase.⁴ The simulation was originally created for a pair of rendezvous demonstrations at Mars planned in the early 2000s, which subsequently were cancelled. It assumes the presence of automated onboard turn and maneuver planning to allow quick turn-around of ground-generated maneuvers or those designed onboard. For ground-based navigation, the model would also assume a great deal of onboard processing, for example of pictures, for reduced turn-around time of solutions and maneuver computations. Figure 11 shows the ensemble control performance in this simulation, showing that over the 250 cases, there was no deviation of more than 10 cm at capture from the desired trajectory.

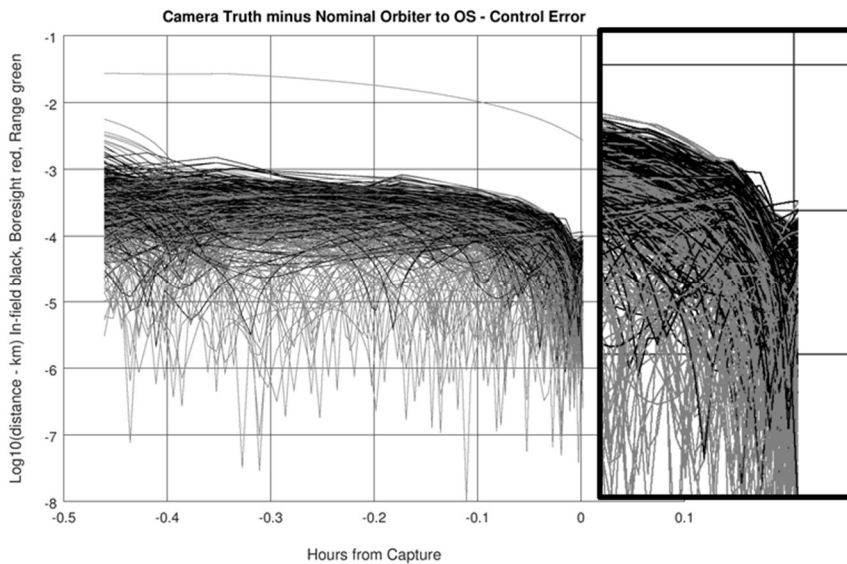


Figure 11. Rendezvous control performance, expected minus nominal, showing no deviation from the approach trajectory greater than 10 cm over 250 cases. The inset shows a close-up of this capture-point performance.

A preliminary conclusion can be made from this simulation that simple passive optical cameras are sufficient for the terminal phase and indeed all phases of the rendezvous. In addition, the same passive optical methodology is applicable to the ground-based navigation that will set up the autonomous capture, for the testing of the autonomy during approach, and for the approach and capture itself. This architecture simplifies and makes more robust the rendezvous and capture methodology.

THE “LOST-IN-SPACE” CONTINGENCY SCENARIO

The above investigation all assumes the nominal case, wherein the SRO is in-place during orbital insertion of the OS and can begin its optical search within the first few hours, before its fast orbital elements can diverge from the expected values. Even if this opportunity is missed, a mosaicking strategy can be used to search for the OS after this diffusion has occurred. However, if the SRO arrives after the OS’s slow elements have diverged from the means, the situation is called a “lost-in-space” contingency scenario. This scenario is so-called as because much of the a priori information about the OS’s orbital elements has been invalidated, leaving only inclination, eccentricity, and SMA unaffected, and placing the OS in a broad latitude band of possible locations around the planet. Using an MRO ONC analog, the presumed historical SRO would have been able to detect the OS at up to 9,000 km range, which was sufficient for even this extreme scenario.^{5,6} The MRO camera, a 1.4 deg, 6-cm aperture reflective telescope, is conservative for this application, especially with a body-fixed camera and long mosaicking times. Even with these assumptions, the SRO was able to find the OS within four weeks. A wider-angle camera (with similar aperture), and/or a gimbal mount would speed this task.

One historical solution to this lost-in-space problem was to outfit the OS with a radio beacon, which could be detected by in-situ assets or by the SRO itself, at greater range and FOV than an optical camera, and in eclipse/backlighting, but at the expense of navigational accuracy and increased hardware complexity of the OS. This subject can be described in-depth, but is not the subject here, so the assumption is made that such an off-nominal lost-in-space contingency scenario is

sufficiently small likelihood that we can ignore it for this part of the analysis. Additionally, terminal rendezvous will always require optical navigation, necessitating an optical suite that may as well be used at range as well. An OS equipped with such a radio beacon would require antenna and radiator surface area, lowering its albedo and thus SNR. For robustness, the 0.35 albedo assumed in this investigation includes this effect, and so one can imagine the performance benefit of optical acquisition if it were to be simply painted white, raising the albedo to approximately 0.9. Complex consequences of a featured OS surface, such as glint and specular reflection, were not considered here.

CONCLUSION

This investigation showed that with currently available passive, visual cameras, a notional robotic sample return orbiter at Mars would be sufficiently capable of detecting and determining the orbital state of an inert non-cooperative orbiting sample canister without the aid of active radio tracking or assistance from other assets. The scheme described would require no cutting-edge technology or expensive/heavy active sensors, such as LIDARs, and is robust to various sources of orbital perturbations, noise, and navigational uncertainties. A reasonable camera suite can determine, before the object can disperse significantly from its nominal state, the relative orbital state to an accuracy sufficient to begin orbit-matching maneuvers and robustly effect a safe rendezvous. Further, the camera suite assumed for this investigation makes many of the improvements suggested by historical “lost-in-space” examination, leading to a superficial conclusion that it would be capable of effecting such a scheme that was marginal for previous cameras. All analyses and simulations presented herein successfully acquire the target while assuming the pessimistic albedo assumptions for an OS with surface features to support electronics, such as a radio beacon, and thus the performance would only improve for a simple passive object painted white.

ACKNOWLEDGMENTS

The authors would like to thank Colin McKinney and Christophe Basset, who were instrumental in selecting camera hardware analogs to meet the requirements of this scheme, and for helping us conclude that rendezvous is not reserved for Earth orbit, active methods, or inter-craft cooperation. Also thanks to the rest of the rendezvous-phase and mission design & navigation working groups without whose feedback this manuscript and indeed investigation overall would be far under-polished. The information presented about potential Mars sample return architectures is provided for planning and discussion purposes only. NASA has made no official decision to implement Mars sample return. This work was carried out at the Jet Propulsion Laboratory, California Institute of Technology, under contract to NASA. Government sponsorship acknowledged.

NOTATION

P_{sun}	[photon/s/m ²]	Photon flux of the sun in the wavelength range of interest (400 nm - 700 nm)
d_{OS}	[m]	Diameter of the OS (assumed spherical)
ρ	[N/A]	Bond albedo of the OS ($0 \leq \rho \leq 1$) in the wavelength range of interest
ϕ	[deg]	Phase angle of the OS (sun-OS-SRO)

$g(\phi)$	[N/A]	Phase function of the OS, describing the distribution of light reflected in a given direction
r	[m]	Range between the SRO and the OS
d_{ap}	[m]	Diameter of camera aperture
θ_{px}	[deg]	Angular size of one pixel
α	[deg/s]	OS apparent motion, as viewed from SRO
n_{px}	[pixel]	Number of central pixels containing the OS during a single image
ψ	[deg]	Angle of OS above the actual Mars surface, as viewed from chaser
t_e	[s]	Exposure time of the image
Q_E	[electron/photon]	Quantum efficiency [typically 0.45 – 0.70]
F_F	[N/A]	Fill factor [typically 0.8 – 1.0]
η_{EO}	[N/A]	Optical throughput [typically 0.6 – 0.8]
$\eta = Q_E F_F \eta_{EO}$	[electron/photon]	Overall camera efficiency (combines other efficiencies)
N_{dark}	[electron/s/pixel]	Dark current noise
N_{read}	[electron/pixel]	Read noise
$N_{stray}(\psi, t_e)$	[electron/pixel]	Stray light noise, as a function of angle above Mars limb and image exposure time.
P_{px}	[photon]	Photons from the OS incident upon the “best” pixel.
N	[electron]	Total noise, from all sources
SNR	[N/A]	Signal-to-noise ratio
E_{sun}	[W/m ²]	Solar irradiance in 400-700 nm
f	[N/A]	General camera efficiency
N	[DN]	General noise term
k	[DN/W]	Power to signal conversion factor

APPENDIX A: NAVIGATION UNCERTAINTIES, 1-SIGMA

Model

Epoch State, Orbiter:	$\sigma = 20.0$ m	$\sigma = 5$ cm/s (spherical)
Epoch State, OS:	$\sigma = 7.0$ km	$\sigma = 2$ m/s (spherical)

Solar pressure (Orbiter only):	$\sigma = 20\%$
Atmosphere drag (Orbiter only):	$\sigma = 25\%$
Twice-daily desats (Orbiter only):	$\sigma = 0.6 \text{ mm/s}$

Measurements

2-way Doppler (continuous when in view):	$\sigma = 0.1 \text{ mm/s}$
OpNavs (RA & Dec):	
NAC:	$\sigma = 1 \text{ as (0.27 mdeg)}$
MAC:	$\sigma = 5 \text{ as (1.25 mdeg)}$

REFERENCES

- ¹ R. C. Woolley, R. L. Mattingly, J. E. Riedel, E. J. Sturm, “Mars Sample Return – Launch and Detection Strategies for Orbital Rendezvous”, AAS 11-519, AAS/AIAA Astrodynamics Specialist Conference, Girdwood, AK, Aug. 2011.
- ² J. N. Maki, C. M. McKinney, R. G. Sellar, R. G. Wilson, D. S. Copley-Woods, D. C. Gruel, D. L. Nuding, M. Valvo, T. Goodsall, J. McGuire, J. Kempenaar, T. E. Litwin, “Enhanced Engineering Cameras (EECAMs) for the Mars 2020 Rover”, 3rd International Workshop on Instrumentation for Planetary Missions, Pasadena, CA, Oct. 2016.
- ³ J. Benito, C. Noyes, R. Shotwell, A. Karp, B. Nakazono, G. Singh, H. Kim, M. Schoenenberger, A. Korzun, M. Lobbia, E. Brandeau, “Hybrid Propulsion Mars Ascent Vehicle Concept Flight Performance Analysis”, IEEE Aerospace Conference, Big Sky, MT, Mar. 2017.
- ⁴ J. E. Riedel, J. Guinn, M. Delpech, J.B. Dubois, D. Geller, P. Kachmar, “A Combined Open-Loop and Autonomous Search and Rendezvous Navigation System For the CNES/NASA Mars Premier Orbiter Mission”, AAS 03-012, 26th Annual AAS Guidance and Control Conference, Breckenridge, CO, Feb. 2003.
- ⁵ M. Adler, W. Owen, J. Riedel, “Use of MRO Optical Navigation Camera to Prepare for Mars Sample Return”, Concepts and Approaches for Mars Exploration, Houston, TX, Jun. 2012.
- ⁶ J. Riedel, A. Vaughan, R. Werner, T. C. Wang, S. Nolet, D. Myers, N. Mastrodemos, A. Lee, C. Grasso, T. Ely, D. Bayard, “Optical Navigation Plan and Strategy for the Lunar Lander Altair; OpNav for Lunar and other Crewed and Robotic Exploration Applications”, AIAA Guidance, Navigation, and Control Conference, Toronto, Ontario, Canada, Aug. 2010.